

# Synthesis and Characterization of Nickel Ferrite/Activated Carbon Nanocomposites as Radar Wave Absorbing Materials at X-Band Frequency

Muhammad Sulthan Ramdhana<sup>1</sup>, Arif Hidayat<sup>1</sup>, Markus Diantoro<sup>1</sup>, Nurul Hidayat<sup>1</sup>, Nur Hanifah<sup>1</sup>, Dahlang Tahir<sup>2</sup>, and Ahmad Taufiq<sup>1,\*</sup>

<sup>1</sup>Department of Physics, Universitas Negeri Malang, Malang, Indonesia.

<sup>2</sup>Department of Physics, Universitas Hasanuddin, Makassar, Indonesia

**Abstract.** In this study, nickel ferrite/activated carbon nanocomposites have been fabricated using iron sand as radar wave absorbing materials at X-Band frequency. The formation of nanocomposites was confirmed by the appearance of Ni, Fe, O, and C elements obtained from the energy dispersive X-ray spectrum, which were the main constituent elements for nickel ferrite and activated carbon. In addition, X-ray diffraction characterization confirmed that the nickel ferrite/activated carbon nanocomposites had an inverse cubic spinel structure and a crystallite size of 11.10 nm. Scanning electron microscopy characterization showed that the nickel ferrite/activated carbon nanocomposites were irregularly spherical with an average particle size of about 46.12 nm. According to the vibrating sample magnetometer characterization, the saturation magnetization of the nanocomposites was 24.26 emu/g with superparamagnetic behavior of the nickel ferrite/activated carbon nanocomposites. Interestingly, the nickel ferrite/activated carbon exhibited a minimum reflection loss of -13.5 dB at a frequency of 7.24 GHz with an effective bandwidth of 1.11 GHz, along with an absorption efficiency higher than 90%. These results indicate that nickel ferrite/activated carbon nanocomposites exhibit promising potential as radar wave absorbing materials at X-band frequency.

## 1 Introduction

Technological advances in electromagnetic waves, including in the fields of wireless communications, satellite navigation systems, and modern defence systems, have progressed rapidly in recent decades [1]. However, new challenges such as electromagnetic interference and radiation leakage can destroy signal stability and weaken the performance of nearby electronic devices. In general, these phenomena can restrict and disturb the performance of radars and communication devices, especially in defence platforms. Therefore, the development of radar-absorbing materials (RAM) become important.

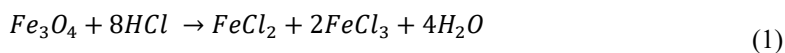
---

<sup>1\*</sup> Corresponding author: [ahmad.taufiq.fmipa@um.ac.id](mailto:ahmad.taufiq.fmipa@um.ac.id)

In general, RAM depends largely on the material's ability to impedance match between the incoming wave and the air [2]. One of the magnetic materials that has been widely studied as a RAM is nickel ferrite. This material offers advantages such as excellent magnetic loss capability, high chemical stability, and a natural resonance frequency suitable for microwave absorption [3]. For example, Fu *et al.* developed a pompon flower morphology from nickel ferrite that produces a minimum reflection loss ( $RL_{\min}$ ) of  $-18.3$  dB [4]. However, the use of single nickel ferrite material shows limitations due to low dielectric loss and conductive loss capabilities that can reduce absorption efficiency. Thus, to improve the absorption performance of nickel ferrite, carbon-based materials are needed, for example, activated carbon. Activated carbon shows great potential in the field of absorber materials because it has various advantages, including high electrical conductivity and good dielectric loss capabilities. In addition, activated carbon generally has a large surface area and a porous structure that allows for interfacial polarization and multiple reflections that can significantly increase the reflection loss value [5]. The combination of these two materials allows for synergy between the magnetic loss mechanisms of nickel ferrite and the dielectric loss of activated carbon, thus supporting its radar wave absorption performance.

## 2. Methods

Nickel ferrite/activated carbon nanocomposites were synthesized by the coprecipitation method using iron sand. The iron sand was first washed thoroughly and separated magnetically using a permanent magnet to obtain  $Fe_3O_4$ . A total of 20 g of pure iron sand that had been separated previously was reacted with HCl (Merck) while continuously stirring to produce a ferric chloride solution, following the method previously reported [6]. The solution contained  $Fe^{2+}$  and  $Fe^{3+}$  ions, following the reaction as shown in Equation (1). The solution was then reacted with nickel  $NiCl_2 \cdot 6H_2O$  (Merk) for 30 min to achieve a homogeneous solution.



Furthermore, activated carbon (dispersed in ethanol) was then reacted with such solution to obtain a new solution. The next step was the dropwise addition of  $NH_4OH$  (Merck) to form a black precipitate. To obtain a neutral pH, the black precipitate was washed with deionized water, then filtered and dried at  $100^\circ C$  for 1 hour. This step was intended to produce nickel ferrite/activated carbon nanocomposites. In this work, the obtained nickel ferrite/activated carbon nanocomposites were characterized by means of X-ray diffraction (XRD) using an X'Pert Pro diffractometer with Cu-K $\alpha$  radiation ( $\lambda = 1.540 \text{ \AA}$ ), Fourier-transform infrared spectroscopy (FTIR, Shimadzu IRPrestige-21), scanning electron microscopy–energy dispersive X-ray spectroscopy (SEM–EDX, FEI Inspect-S50), vibrating sample magnetometer (VSM, Quantum Design PPMS® VersaLab™ Cryogen-Free), and vector network analyzer (VNA).

## 3. Results and Discussion

The XRD pattern in the range of  $2\theta = 10^\circ$ – $90^\circ$  for the nickel ferrite/activated carbon nanocomposites is depicted in Figure 1. The observed diffraction peaks at  $2\theta = 30.33^\circ$  (220),  $35.68^\circ$  (311),  $43.35^\circ$  (400),  $53.78^\circ$  (422),  $57.43^\circ$  (511),  $62.87^\circ$  (440), and  $74.40^\circ$  (533) correspond to the cubic spinel structure of nickel ferrite with a face-centered cubic (FCC) lattice, respectively, confirming the previous work [7]. In general, additional peaks were not detected, demonstrating that the nanocomposites were dominated by the spinel structure owing to nickel ferrite. The clear peaks of activated carbon were not observed, showing the formation of an amorphous phase. Interestingly, the presence of activated carbon did not shift in the ferrite diffraction peaks. This

phenomenon indicates that incorporation of activated carbon occurs via physical interactions without substitution of carbon into the spinel lattice.

The diffraction data for the nanocomposites were quantitatively analyzed using a refinement, employing AMCSD 0007394 as the reference model. The data analysis showed that nickel ferrite/activated carbon nanocomposites had lattice parameters  $a = b = c = 8.3606 \text{ \AA}$ , supporting the findings of Raj *et al.* [8]. The relatively good agreement between the observed and calculated patterns indicates a high degree of crystallinity of the nickel ferrite phase. The absence of significant lattice parameter deviations indicates that the addition of activated carbon does not cause substantial lattice distortion or strain in the refinement detection capability. Meanwhile, the crystal size of the nanocomposite was also calculated by the Debye-Scherrer equation in Equation 2 [9].

$$D = \frac{k\lambda}{\beta \cos\theta} \quad (2)$$

Where  $k = 0.9$ ,  $\lambda = 1.5406 \text{ \AA}$  (Cu-K $\alpha$  radiation),  $\theta$  is the angle, and  $\beta$  is the peak width at half height (FWHM). Based on the calculation result, nickel ferrite is known to have a crystallite size of 11.10 nm.

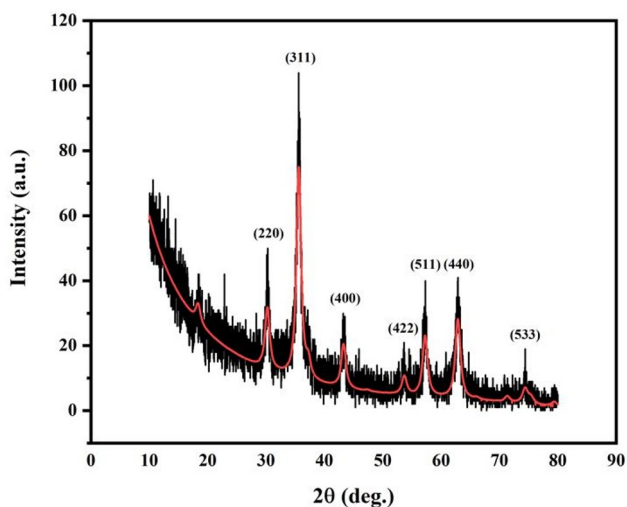


**Fig. 1.** Diffraction pattern of nickel ferrite/activated carbon nanocomposites

The FTIR spectrum of nickel ferrite/activated carbon nanocomposites is shown in Figure 2. The broad absorption band of around  $3440 \text{ cm}^{-1}$  is attributed to the stretching vibration of O–H groups of water molecules adsorbed on the particle surface and the  $\text{CO}_2$  vibration at  $2311 \text{ cm}^{-1}$ . The band at  $1633 \text{ cm}^{-1}$  is attributed to the stretching vibration of C=C bonds originating from aromatic groups. In addition, the band at  $1536 \text{ cm}^{-1}$  is associated with the stretching vibration of carbonyl groups C=O, which is a typical functional group of activated carbon. The absorption band observed at  $1537 \text{ cm}^{-1}$  is attributed to the N–O functional group. The peak at  $1360 \text{ cm}^{-1}$  is from the C–N bond of aromatic amines. The peaks at  $596 \text{ cm}^{-1}$  and  $415 \text{ cm}^{-1}$  are attributed to the vibration of Fe–O at tetrahedral sites and Ni–O–Fe vibrations at octahedral sites, respectively [10]. The presence of these two bands confirms that nickel ferrite has been well formed during the coprecipitation process.

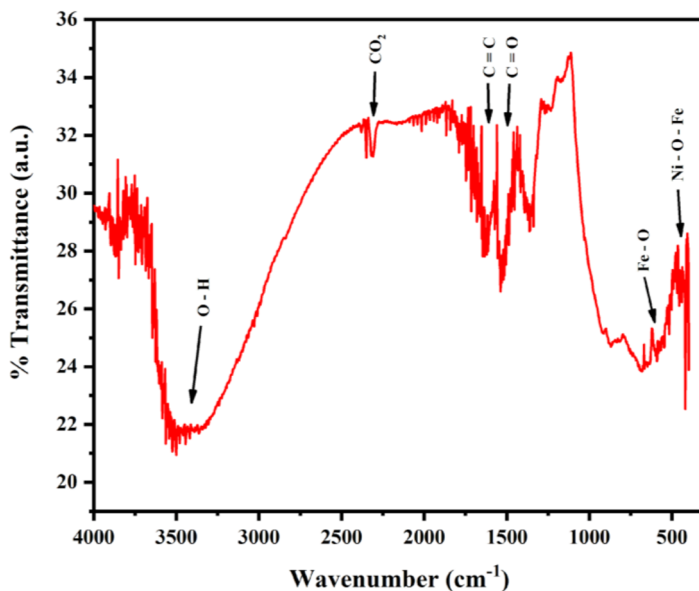


**Fig. 2.** FTIR spectrum of nickel ferrite/activated carbon nanocomposites

The results of surface morphology observations using scanning electron microscopy with a magnification of 50,000 $\times$  are shown in Figure 3. The activated carbon surface displays a typical porous morphology, but some pores appear not to be fully open. The activated carbon exhibits an irregular and porous surface morphology, while nickel ferrite nanoparticles are observed to be attached and distributed on the carbon surface. This condition is caused by the formation of aggregations of nickel ferrite nanoparticles that are attached and distributed unevenly on the activated carbon surface. The aggregation of nickel ferrite particles occurs due to the presence of van der Waals forces and interactions between magnetic dipoles [11]. In this study, the quantitative characteristics of the nickel ferrite/activated carbon nanocomposites surface were analyzed. The analysis results indicate an average particle size of approximately 46.12 nm.

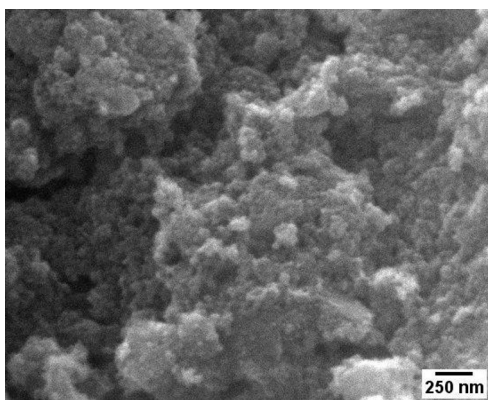


**Fig. 3.** Morphology and particle size distribution of nickel ferrite/activated carbon nanocomposites

The magnetization curve obtained through vibrating sample magnetometer characterization is shown in Figure 4. Qualitatively, the magnetization curve of nickel ferrite/activated carbon nanocomposites shows superparamagnetic behavior characterized by a narrow *S*-shaped curve without wide hysteresis [12]. This is also confirmed through the results of Langevin model fitting,

which reveals the coercivity ( $H_c$ ) and remanent magnetization ( $M_r$ ) values of 0.0028 T and 24.26 emu/g, respectively, indicating superparamagnetic characteristics [13]. Meanwhile, the saturation magnetization ( $M_s$ ) value of nickel ferrite/activated carbon reaches 24.26 emu/g. This result is lower than pure nickel ferrite obtained from research by Fröhlich *et al.*, which has a  $M_s$  of 41.19 emu/g [14]. This decrease in the  $M_s$  value is caused by the presence of activated carbon, which is non-magnetic, so that when incorporated with nickel ferrite, it reduces the magnetization value.

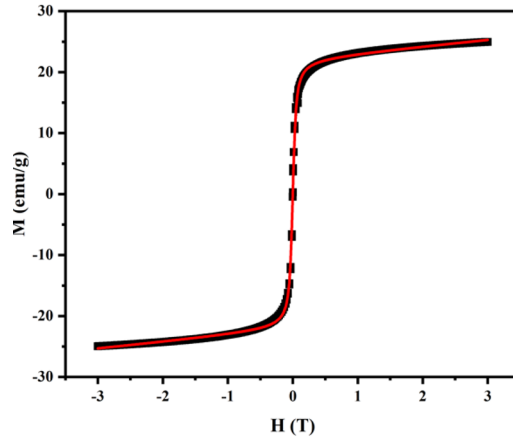


**Fig. 4.** Hysteresis curve of nickel ferrite/activated carbon nanocomposites

The performance of electromagnetic wave absorbing materials was measured using vector network analysis in the frequency range of 7–13 GHz with a sample thickness of 5 mm. The minimum reflection loss value shows the material's ability to absorb electromagnetic energy, calculated using Equations (3)–(4) [15].

$$\text{Absorption Efficiency (\%)} = 100 \times (1 - |\Gamma|^2) \quad (3)$$

$$\Gamma = \left( \frac{RL(\text{dB})}{20} \right) \quad (4)$$

Based on the calculation of absorption efficiency calculated using Equation (2)–(3), the  $RL_{min}$  value is equivalent to an absorption efficiency of more than 90%, which means that nickel ferrite/activated carbon is able to absorb most of the electromagnetic energy. This absorption behavior is caused by a combination of electromagnetic losses from both constituent materials. Magnetic losses in nickel ferrite particles are mainly caused by magnetic spin resonance and domain relaxation, while dielectric losses consist of interfacial polarization and conductive losses originating from the alternating current of the activated carbon. In addition, the porous structure of the activated carbon receives many reflections on the material and lengthens the wave propagation path, which increases the opportunity for absorbed energy. The nickel ferrite/activated carbon nanocomposites have  $RL_{min} = -13.5$  dB and an efficiency higher than 90%. The nickel ferrite/activated carbon nanocomposites show promising potential as an efficient and environmentally friendly radar wave absorbing materials.

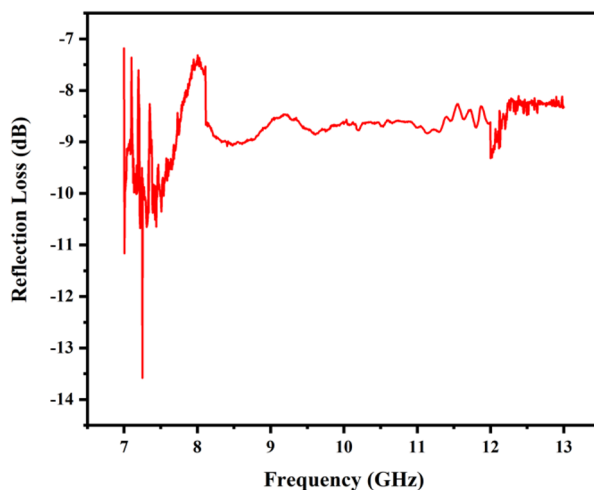


Fig. 5. Reflection loss of nickel ferrite/activated carbon nanocomposites

## 4. Conclusion

Nickel ferrite/activated carbon nanocomposites have been synthesized using a coprecipitation method with natural iron sand as the main precursor source. X-ray diffraction characterization results confirmed the formation of nickel ferrite spinel with a crystal size of 11.10 nm. Based on the resulting infrared spectrum, the presence of Fe–O and Ni–O–Fe bond vibrations was found, indicating the presence of nickel ferrite, as well as C=C bonds which were characteristic of activated carbon. Furthermore, the nickel ferrite/activated carbon nanocomposites exhibited irregular morphology with a particle size of 46.12 nm. Magnetization test results showed that the nanocomposites had superparamagnetic properties with an  $M_s$  value of 24.26 emu/g. Electromagnetic absorption performance tests revealed that the nickel ferrite/activated carbon nanocomposites were able to produce an  $RL_{min}$  value of  $-13.5$  dB at a frequency of 7.24 GHz, equivalent to an absorption efficiency of more than 90%. Overall, these results indicate that nickel ferrite/activated carbon nanocomposites have high potential as efficient, environmentally friendly radar wave absorbing materials and support the concept of sustainable materials.

## Acknowledgment

This work was supported by “Hibah Tesis” from Universitas Negeri Malang with contract number 4.4.557/UN32.14.1/LT/2024.

## References

- [1] Y. Zhang, G. Li, S. Ma, Z. Li, F. Fan, and Y. Huang, “Switchable Multi-Spectral Electromagnetic Defense in the Ultraviolet, Visible, Infrared, Gigahertz, and Terahertz Bands Using a Magnetically-Controllable Soft Actuator,” *ACS Nano*, vol. 19, no. 11, pp. 11295–11308, Mar. 2025, doi: 10.1021/acsnano.5c00138.
- [2] Y. Zhang, H. Si, S. Liu, Z. Jiang, J. Zhang, and C. Gong, “Facile synthesis of BN/Ni nanocomposites for effective regulation of microwave absorption performance,” *J. Alloys Compd.*, vol. 850, p. 156680, Jan. 2021, doi: 10.1016/j.jallcom.2020.156680.

- [3] C. Wang, N. Chen, Y. Xiao, J. He, R. Han, and N. Song, "Exceeding natural resonance frequency limit and enhanced microwave absorption performance of Fe<sub>3</sub>O<sub>4</sub> nanorods coated with SiO<sub>2</sub> layer," *Ceram. Int.*, vol. 49, no. 22, pp. 36233–36243, Nov. 2023, doi: 10.1016/j.ceramint.2023.08.304.
- [4] M. Fu *et al.*, "Multifunctional pompon flower-like nickel ferrites as novel pseudocapacitive electrode materials and advanced absorbing materials," *Ceram. Int.*, vol. 46, no. 1, pp. 850–856, Jan. 2020, doi: 10.1016/j.ceramint.2019.09.042.
- [5] Y. Chen *et al.*, "Fe<sub>3</sub>C/Fe implanted hierarchical porous carbon foams for lightweight and broadband microwave absorption," *Diam. Relat. Mater.*, vol. 142, p. 110738, Feb. 2024, doi: 10.1016/j.diamond.2023.110738.
- [6] W. P. Agista *et al.*, "Exploring the role of Mn<sup>2+</sup> in the structure, magnetic properties, and radar absorption performance of Mn<sub>x</sub> Fe<sub>3-x</sub>O<sub>4</sub>-DEA/MWCNT nanocomposites," *RSC Adv.*, vol. 13, no. 42, pp. 29332–29341, 2023, doi: 10.1039/D3RA05333D.
- [7] S. G. Divakara, B. Mahesh, B. K. Jayanna, and H. G. Anil Kumar, "Photocatalytic degradation of crystal violet dye using honey mediated synthesis of NiFe<sub>2</sub>O<sub>4</sub> nanoparticles," *Green Chem. Lett. Rev.*, vol. 18, no. 1, p. 2543931, Dec. 2025, doi: 10.1080/17518253.2025.2543931.
- [8] R. Raj, S. K. Paswan, L. Kumar, G. Prasad Singh, and K. K. Haldar, "Ti<sub>3</sub>C<sub>2</sub>T<sub>x</sub> Nanosheet/NiFe<sub>2</sub>O<sub>4</sub> Nanoparticle Composites for Electrocatalytic Water Splitting," *ACS Appl. Nano Mater.*, vol. 8, no. 3, pp. 1649–1662, Jan. 2025, doi: 10.1021/acsanm.4c06758.
- [9] A. Taufiq, R. Sutiami, S. U. I Subadra, A. Hidayat, M. Diantoro, S. Sunaryono, N. Hidayat, and W. A. Adi, "Radar Absorption Performance of Fe<sub>3</sub>O<sub>4</sub>/AC/PANI Nanocomposites Prepared from Natural Iron Sand," *Int. J. Eng.*, vol. 33, no. 2, Feb. 2020, doi: 10.5829/ije.2020.33.02b.15.
- [10] I. F. F. Christopher, A. Karuppiyah, V. G. Thanapalan, A. V. Selestin, and T. Suyambu, "Preparation of SiO<sub>2</sub> Nano Matrix Engendered from Coal Fly Ash Encrusted with NiFe<sub>2</sub>O<sub>4</sub> Nanocomposites for High Electrochemical Performance," *Silicon*, vol. 16, no. 1, pp. 157–176, Jan. 2024, doi: 10.1007/s12633-023-02656-4.
- [11] A. A. Kuznetsov and A. F. Pshenichnikov, "Sedimentation equilibrium of magnetic nanoparticles with strong dipole-dipole interactions," *Phys. Rev. E*, vol. 95, no. 3, p. 032609, Mar. 2017, doi: 10.1103/PhysRevE.95.032609.
- [12] A. Bajorek *et al.*, "Tuning Physical Properties of NiFe<sub>2</sub>O<sub>4</sub> and NiFe<sub>2</sub>O<sub>4</sub>@SiO<sub>2</sub> Nanoferrites by Thermal Treatment," *Metall. Mater. Trans. A*, vol. 53, no. 4, pp. 1208–1230, Apr. 2022, doi: 10.1007/s11661-021-06567-0.
- [13] A. Taufiq, S. U. I. Subadra, N. Hidayat, E. Handoko, M. Alaydrus, and L. Chuenchom, "Eco-Friendly Fabrication of Fe<sub>3</sub>O<sub>4</sub>/MWCNT/ZnO Nanocomposites from Natural Sand for Radar Absorbing Materials," 2021.
- [14] A. C. Fröhlich, E. L. Foletto, and G. L. Dotto, "Preparation and characterization of NiFe<sub>2</sub>O<sub>4</sub>/activated carbon composite as potential magnetic adsorbent for removal of ibuprofen and ketoprofen pharmaceuticals from aqueous solutions," *J. Clean. Prod.*, vol. 229, pp. 828–837, Aug. 2019, doi: 10.1016/j.jclepro.2019.05.037.
- [15] N. Hanifah *et al.*, "A novel Fe<sub>3</sub>O<sub>4</sub>/ZnO/PANI/rGO nanohybrid material for radar wave absorbing," *Mater. Chem. Phys.*, vol. 317, p. 129169, Apr. 2024, doi: 10.1016/j.matchemphys.2024.129169.